

See discussions, stats, and author profiles for this publication at: <https://www.researchgate.net/publication/236783923>

Equilibrium and Growth Morphology of Oligothiophenes: Periodic Bond Chain Analysis of Quaterthiophene and Sexithiophene Crystals

ARTICLE in CRYSTAL GROWTH & DESIGN · MARCH 2013

Impact Factor: 4.89 · DOI: 10.1021/cg301868m

CITATIONS

6

READS

43

4 AUTHORS, INCLUDING:



Francesco Roberto Massaro

University of Padova

41 PUBLICATIONS 286 CITATIONS

[SEE PROFILE](#)



Marco Bruno

Università degli Studi di Torino

84 PUBLICATIONS 704 CITATIONS

[SEE PROFILE](#)



Dino Aquilano

Università degli Studi di Torino

184 PUBLICATIONS 992 CITATIONS

[SEE PROFILE](#)

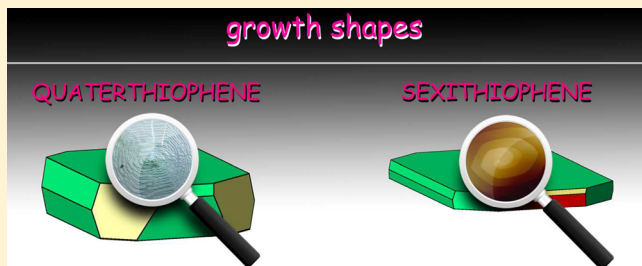
Equilibrium and Growth Morphology of Oligothiophenes: Periodic Bond Chain Analysis of Quaterthiophene and Sexithiophene Crystals

Francesco Roberto Massaro,^{*,†,‡} Massimo Moret,[†] Marco Bruno,[‡] and Dino Aquilano[‡]

[†]Dipartimento di Scienza dei Materiali, Università di Milano Bicocca, via R. Cozzi 53, I-20125 Milano, Italy

[‡]Dipartimento di Scienze della Terra, Università di Torino, via Valperga Caluso 35, I-10125 Torino, Italy

ABSTRACT: The athermal ($T = 0$ K) equilibrium and growth crystal shapes of two members of the oligothiophenes series, namely, quaterthiophene and sexithiophene, were simulated *in vacuo* by using the UNI and UFF empirical potentials. By applying the Hartman–Perdok method of the periodic bond chains (PBC), the surface profiles were obtained, providing the specific surface and attachment energy values, both for bulk-like and relaxed surfaces. Calculations demonstrate that surface relaxation weakly affects surface and, even more, attachment energies of such semiconductor molecular crystals. The two phases show analogous features: barrel-like equilibrium shapes for both quaterthiophene and sexithiophene, and plate-like growth shapes, in particular, in the sexithiophene case.



1. INTRODUCTION

Organic molecules with extended electronic π -conjugation have been investigated during several years in relation to their semiconducting properties when in crystalline form.^{1–4} They are expected in the future to represent a valid substitute for inorganic semiconductors in electronics applications. Studies on these organic materials are conducted either on single crystals and thin films, aiming at understanding their intrinsic properties and best performance of operating devices.^{5–8} Charge transport properties of optoelectronic devices based on organic crystalline materials are closely linked with crystal and thin-film morphology; thus considerable experimental efforts have been devoted to control morphologies for optimizing device performance. As an example, it is now established that grain boundaries in organic thin film transistors may act as traps for charge carriers.⁹ Similarly surface energies, which are experimentally hardly accessible, are main actors on determining film and crystal morphology as well as contact planes in thin film heterostructures.¹⁰ Hence, support from theoretical modeling can help to better understanding intermolecular interactions within crystals^{11,12} as well as in heteroepitaxial systems.^{13–17}

A fundamental support to this purpose comes from a thorough analysis of the role of the crystal structure on determining the crystal morphology. Recently, a few papers have dealt with the simulation of surface energies and equilibrium crystal morphology for organic semiconductors chosen among acenes, oligothiophenes, and polyphenylenes.^{18–22} However, as already pointed out in previous papers on this topic,^{11,12} there was no systematic approach for determining all possible forms involved in equilibrium crystal morphologies nor for properly considering growth morphology. Indeed, only a biased choice of “easy faces”, that is, those having

simple and low indexes, was considered, leading to greatly oversimplified predicted morphologies for all the crystal materials studied.

These results motivated us to calculate the surface energies of the most relevant semiconducting organic crystalline materials. The present work is part of systematic studies dedicated to the prediction of equilibrium and growth morphology of molecular crystals.^{11,12} Our approach is based on the detailed analysis and classification of the intermolecular interactions in crystals, together with the definition of the character of the crystal faces according to the periodic bond chain (PBC) theory developed by Hartman and Perdok,^{23–25} supported by computer simulations with empirical potentials.

Calculations about acenes proved that, for both the theoretical equilibrium and growth shapes, it is sufficient to take into account the molecular interactions belonging to the first order of magnitude and all the related PBC ranks.¹¹ We extend here this systematic approach to the study of organic systems belonging to the oligothiophenes class, which were among the first organic systems selected as potential semiconductors, namely quaterthiophene (4T)²⁶ and sexithiophene (6T).²⁷ We provide an estimate of equilibrium and growth crystal shapes for the two compounds together with the predicted shape of the two-dimensional critical nuclei forming onto the basal faces. The results of the simulations were compared with experimental crystal morphologies. This study led us to unravel that even in the presence of strong similarities between these two homologues there are also differences that cannot emerge with a more simple approach. Experimental

Received: December 23, 2012

Revised: January 20, 2013

Published: January 22, 2013



studies of the morphology of UHV evaporated 4T and 6T thin films on various substrates indicate that the crystals tend to be oriented so that the 4T {001} or 6T {100} forms are parallel to the substrate. It is shown here that these surfaces have the lowest surface energy among the numerous faces found in our PBC analysis, owing to the stronger intermolecular bonds between molecules in the herringbone layer compared to those between molecules in adjacent layers. This anisotropy in the bonding net is the key for the films to usually exhibit {001} or {100} surfaces, for 4T and 6T, respectively, as contact plane in organic–organic heterostructures.^{13,16,17,28,29}

2. COMPUTATIONAL DETAILS

On the basis of our previous results with the simulation of crystal morphology of organic semiconductors,^{11,12} different computer codes coupled to two different sets of empirical potentials were used to perform the calculations. The two computer codes adopted are described immediately below.

(i) The CSEHP (Crystal Site Energy according to Hartman and Perdok^{30,31}) program is a homemade code. We chose to include the UNI^{32,33} force field in our code, mainly to evaluate the intermolecular interactions and the end chain energy (ECE) of the PBCs, namely, the energy released when a molecule enters, in a crystallographic position, at one end of a semi-infinite PBC.

(ii) The other set of calculations, mainly optimization of slab geometries, specific surface energy (γ_{hkl}), and attachment energy (E_{att}^{hkl}) estimates, were carried out by using the UFF³⁴ molecular potentials implemented in the GULP 3.4 package (General Utility Lattice Program).³⁵ Bulk and slab geometry optimizations were performed by means of the Newton–Raphson method and considered converged when the gradient tolerance and the function tolerance ($gtol$ and $ftol$ adimensional parameters in GULP) were smaller than 0.0001 and 0.00001, respectively.

All surfaces were studied by using the 2D-slab model³⁶ where (hkl) slabs of varying thickness were obtained by cutting the bulk structure along the plane of interest. Calculations were performed by considering the original 1×1 surface cell and the slab divided into two regions:

Region 1, containing both the surface and the underlying layers that are allowed to relax;

Region 2, having the same number of layers as region 1 and containing the rest of the material's slab where no relaxation, with respect to the bulk crystal structure, is assumed to occur.

Calculations were done by considering slabs with thickness up to 10 layers (five for each region), which are sufficient to reproduce bulk-like properties at the center of the slab and to obtain a careful description of the surface.

The γ_{hkl} values were estimated from the energy of the surface block (U_s , region 1) and the energy of a portion of bulk crystal (U_b , region 2) containing the same number of atoms as the surface block.³⁷ Both energies are referred to A_{hkl} the common surface area of the primitive unit cell:

$$\gamma_{hkl} = (U_s - U_b)/A_{hkl}$$

E_{att}^{hkl} was calculated by adopting the following relation:

$$E_{att}^{hkl} = U_{tot}^{n+1} - U_{tot}^n - U_{tot}^1$$

where U_{tot}^n is the total internal energy of a surface model consisting of n growth layers, while U_{tot}^1 is the energy of the growth layer alone.

3. METHODOLOGY

We used a multistage approach previously devised and validated.^{11,12} The whole procedure is grounded on the PBC analysis after Hartman and Perdok^{23–25} which aims at identifying within a crystal structure [uvw] crystallographic directions characterized by strong interactions among molecules (growth units of the crystal). Such directions define and

rule the character of the $\{hkl\}$ forms, which can be F (flat), S (stepped), or K (kinked), depending on the number of PBCs running within a slice of thickness d_{hkl} allowed by the extinction rules, which in turn controls the morphology of a crystal.^{23,24}

During the first stage, the molecular interactions inside the crystal bulk are evaluated and then arranged according to different “bond orders” starting from the strongest interaction down to the less energetic ones. Capitalizing on the results of our study about acenes,^{11,12} we take into account just the molecular interactions belonging to the first order of magnitude (see Figure 1), that is, those ranging from the strongest interaction down to the one involving 10% of the highest interaction energy.

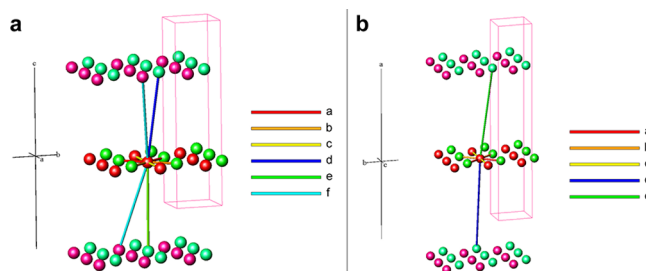


Figure 1. The first bond order graph describing the crystal structure of 4T (a) and 6T (b). Intermolecular bonds are defined in Tables 1 and 4, respectively. The schemes report only the barycenters of the molecules for the sake of simplicity and reflect the portion of crystal structure considered to estimate the molecular interactions.

In the second stage, the existence and composition of PBCs inside the bulk structure are revealed starting from the $[uvw]$ directions determined by the strongest intermolecular bonds and completing the analysis with PBCs built by more than one intermolecular interaction. Subsequently, the ECEs are calculated for each PBC and a hierarchy based on the ECE order of magnitude is set (“PBC rank” hereinafter). All the $\{hkl\}$ crystallographic forms arising from the identified PBCs, are then given the characters F, S, or K. Afterward, starting from the first PBC rank, F_1 , S_1 , and K_1 forms are identified, followed by forms described by periodic chains of lower rank.

In the final stage, γ_{hkl} values are calculated by means of GULP-UFF in order to model the equilibrium shapes (bulk-like and relaxed). The same program-force field couple allowed us to quantify E_{att}^{hkl} as well, by which approximate linear growth rates (R^{hkl}) for each crystal form could be estimated, according to the relation: $R^{hkl} \propto E^{hkl}$.³⁸

Before facing the calculation results and the related discussion, it is worth recollecting the reasons why we adopted the “free way” mentioned above for searching the PBCs.

First of all, the only constraints for a PBC required by the HP method are (i) stoichiometry of the bond chain, (ii) periodicity and continuity along the chain development, (iii) lack of electric dipole moment perpendicular to the chain axis. It ensues that the “thickness” of the chain is not relevant in itself. However, the constraints on the chain thickness become important only when one has to decide on the character of a given face; in that case, the thickness of the PBC cannot be larger than the thickness of the slice d_{hkl} allowed by the extinction rules of the space group of the crystal.

A typical example is that of a flat (F) face: a given (hkl) face can assume F character (and hence it can grow layer-by-layer) only if two nonparallel PBCs run “within” the corresponding

d_{hkl} slice. In the frame of the HP method one can predict the normal growth rate of this kind of face by calculating its attachment energy E_{att}^{hkl} , which is the energy, per formula unit, released when an allowed d_{hkl} layer deposits and spreads on the pre-existing face; consequently, the E_{att}^{hkl} value is strictly related to the structure of the PBCs determining the thickness of the slice.

The evaluation of the equilibrium shape (ES) of a crystal is markedly less constraining, as far as it concerns the structure and the thickness of the PBCs. As a matter of fact, the ES depends on the ratio between the values of the specific free energies γ_{hkl} of the different $\{hkl\}$ crystal forms; values, according to the Born–Stern definition, are related, in turn, to the separation work (Abtrennungarbeit) of two semi-infinite and equivalent slabs along a given separation surface. In this case the thickness of the slab does not correspond to the elementary d_{hkl} slice; on the contrary, it is theoretically semi-infinite as well, even if a finite number of d_{hkl} slices is sufficient to obtain a rapid convergence of the γ_{hkl} value. In other words, the evaluation of γ_{hkl} does not depend on the constraints imposed by the systematic extinction rules, but only on the shape of the profile adopted as a separation surface. To do that one can use whatever method, even if the experience plays in favor of the HP approach, without applying the constraint of the thickness of the PBCs running parallel to the separation surface.

Summing up, these are the reasons why to choose the PBCs with the largest freedom to evaluate the equilibrium shape of our crystals and limit our choice of PBCs in the frame of the strict application of the extinction rules.

4. RESULTS AND DISCUSSION

4.1. The Equilibrium Shape. Starting from the crystal structures of the low temperature polymorphs of quaterthiophene (space group $P2_1/c$; $a_0 = 6.085$, $b_0 = 7.858$, $c_0 = 30.483$ Å; $\beta = 91.81^\circ$, $Z = 4$)²⁶ and sexithiophene (space group $P2_1/n$; $a_0 = 44.708$, $b_0 = 7.851$, $c_0 = 6.029$ Å; $\beta = 90.76^\circ$, $Z = 4$),²⁷ we calculated the surface energies for all the $\{hkl\}$ forms originated from the appropriate PBCs. Utilizing them in the Gibbs–Wulff's construction,³⁹ the corresponding crystal ES were obtained (Figures 2 and 3).

4.1.1. Quaterthiophene (4T). When considering the first order intermolecular bonds,¹¹ it is possible to number 6 van der Waals (vdW) interactions (Table 1 and Figure 1a) and 12 PBCs (Table 2) in the 4T crystal structure. In Table 2 the ECEs of these PBCs, calculated with CSEHP, are reported;

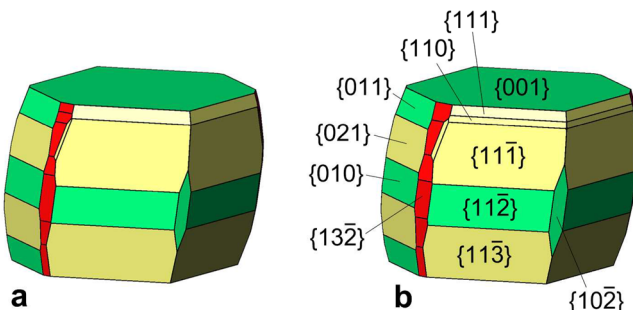


Figure 2. Quaterthiophene equilibrium shapes from calculations performed by means of UFF without (a) and with surface relaxation (b). Drawing (b) reports indexes only for those crystallographic forms having MRI $\geq 1.0\%$.

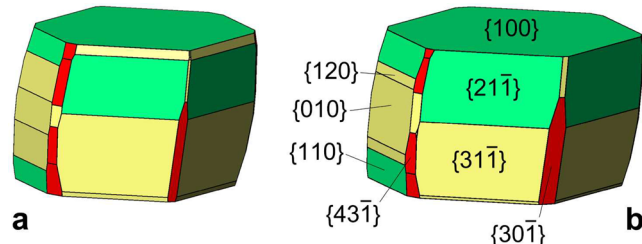


Figure 3. Sexithiophene equilibrium shapes from calculations performed by means of UFF without (a) and with surface relaxation (b). Drawing (b) reports indexes only for those crystallographic forms having MRI $\geq 1.0\%$.

Table 1. Molecular Interactions Issued from the First Bond Order in 4T^a

molecule	molecule in the shifted cell	distance [Å]	direction	interaction [kJ/mol]	bond label
1, 3	2, 4	4.933	[0 0 0]	-52.2	a
1, 3	2, 4	5.007	[1 0 0]	-51.8	b
1, 2, 3, 4	1, 2, 3, 4	6.085	[1 0 0]	-37.5	c
1, 2	4, 3	15.547	[1 0 0]	-8.7	d
1, 2	4, 3	15.413	[0 01̄]	-8.6	e
1, 2	3, 4	16.494	[1̄0 0]	-7.4	f

^aThe calculations were performed by means of program-potential CSEHP-UNI.

Table 2. PBC End Chain Energies (ECEs) Relative to the First Bond Order Intermolecular Interactions in 4T^a

PBC	PBC rank	bonds	ECE [erg/molecule]
[1 0 0]	1	a + b + c + d + e + f	-1.22×10^{-12}
[0 1 0]	1	a + b + d + e + f	-5.64×10^{-13}
[1 1 0]	1	a + b + d + e	-4.99×10^{-13}
[0 0 1]	2	a + e	-9.90×10^{-14}
[2 0 1]	2	a + d + f	-9.90×10^{-14}
[1 0 1]	2	a + b + d + e + f	-7.85×10^{-14}
[2 1 1]	2	a + d + f	-7.84×10^{-14}
[1 1 1]	2	a + e + f	-6.44×10^{-14}
[1 1 2]	2	a + b + d + e + f	-5.00×10^{-14}
[3 1 0]	2	a + b + c + d + e	-4.86×10^{-14}
[0 1 1]	2	a + e	-4.84×10^{-14}
[3 1 2]	4	a + b + d + e + f	-5.55×10^{-16}

^aThe “bonds” column shows the name of the intermolecular bonds forming the PBCs.

three of them belong to the first, eight to the second and a very weak chain to the fourth PBC rank.

Thirty-one crystallographic forms are generated from the set of 12 PBCs, of which the F, S, and K forms are 6, 10, and 15, respectively. Table 3 shows the 31 forms classified and ordered according to their PBC rank and specific surface energy. The energy difference percentage: $\Delta_{UR} = (\gamma_{relaxed} - \gamma_{unrelaxed})/\gamma_{unrelaxed}$ between relaxed and unrelaxed surfaces is also indicated for all forms. It is worth outlining the weak relaxation suffered by the surfaces: indeed, Δ_{UR} goes from a minimum of 1.2% for the {001} form, to a maximum difference of 3.3% in the {311} case.

Figure 2 clearly outlines that both the bulk-like (unrelaxed) and the relaxed ES show {001} as the prevailing form and several secondary faces nearly perpendicular to it, from which a barrel-like habit.

Table 3. Quaterthiophene Specific Surface and Attachment Energies for the 31 Crystallographic Forms Arising from First Bond Order Interactions^a

character	form	$\gamma_{\text{unrelaxed}}$	γ_{relaxed}	$\Delta_{\text{UR}} (\%)$	$E_{\text{att}}^{\text{unrelaxed}}$	$E_{\text{att}}^{\text{relaxed}}$	$\Delta_{\text{EAR}} (\%)$
F ₁	{0 0 1}* [*]	90.2	89.1	-1.2	-25.7	-25.7	0.0
S ₂	{1 1 $\bar{3}$ }*	112.7	110.5	-2.0	-108.1	-107.9	-0.1
F ₂	{1 1 $\bar{2}$ }*	113.7	111.2	-2.2	-104.5	-104.3	-0.2
F ₂	{0 1 0}* [*]	114.5	113.0	-1.3	-95.0	-95.0	-0.1
S ₂	{0 2 1}* [*]	116.1	114.4	-1.5	-107.3	-107.1	-0.2
S ₂	{1 1 $\bar{1}$ }*	118.5	116.3	-1.9	-105.8	-105.7	-0.2
F ₂	{0 1 1}* [*]	121.3	119.4	-1.6	-76.4	-76.4	0.0
K ₂	{1 3 $\bar{2}$ }*	123.4	121.0	-1.9	-166.0	-168.3	1.4
K ₂	{1 3 $\bar{3}$ } [*]	124.1	121.4	-2.2	-166.8	-169.4	1.6
S ₂	{1 2 $\bar{2}$ } [*]	125.7	122.9	-2.2	-139.7	-140.7	0.8
K ₂	{1 3 $\bar{1}$ } [*]	125.8	122.9	-2.3	-165.8	-168.8	1.8
K ₂	{1 3 $\bar{4}$ } [*]	127.0	124.2	-2.2	-168.3	-171.1	1.6
K ₂	{1 3 $\bar{5}$ } [*]	127.1	124.7	-1.9	-169.4	-171.9	1.5
K ₂	{1 3 0} [*]	130.3	127.6	-2.1	-167.8	-170.4	1.6
S ₂	{1 2 0} [*]	131.0	128.2	-2.1	-138.5	-139.7	0.9
K ₂	{1 3 1} [*]	131.3	128.6	-2.1	-167.6	-170.4	1.7
S ₂	{1 1 0}* [*]	131.7	128.7	-2.3	-100.9	-100.6	-0.3
F ₂	{1 0 $\bar{2}$ }*	136.1	132.4	-2.7	-96.7	-96.2	-0.5
K ₂	{1 3 2} [*]	135.5	133.2	-1.7	-170.7	-172.8	1.3
S ₂	{2 1 $\bar{3}$ } [*]	137.1	133.4	-2.7	-139.0	-140.8	1.3
K ₄	{3 1 $\bar{5}$ } [*]	139.4	134.9	-3.2	-168.6	-173.2	2.7
K ₂	{1 3 3} [*]	139.6	136.3	-2.4	-171.1	-174.6	2.0
S ₂	{1 1 1}* [*]	141.4	138.9	-1.8	-117.5	-117.5	0.0
K ₄	{3 1 $\bar{4}$ } [*]	143.2	139.1	-2.9	-169.0	-172.6	2.1
K ₄	{2 0 $\bar{3}$ } [*]	144.6	140.6	-2.8	-161.4	-164.8	2.1
S ₂	{2 1 $\bar{1}$ } [*]	148.9	144.6	-2.9	-142.6	-144.6	1.4
S ₂	{1 0 $\bar{1}$ } [*]	150.2	146.6	-2.4	-121.4	-122.0	0.5
K ₂	{3 1 $\bar{2}$ } [*]	153.0	148.4	-3.0	-169.9	-174.0	2.4
K ₂	{3 1 $\bar{1}$ } [*]	158.3	153.1	-3.3	-172.8	-178.2	3.1
K ₂	{2 0 $\bar{1}$ } [*]	159.9	155.5	-2.8	-168.5	-172.6	2.5
F ₂	{1 0 0} [*]	166.8	162.6	-2.5	-108.8	-108.2	-0.5

^aValues are calculated by means of UFF, expressed respectively in erg/cm² and kJ/mol, and ordered by relaxed γ values. Forms with MRI $\geq 1.0\%$ are quoted with an asterisk.

We code by color the crystal faces according to their character (green for F, yellow for S, and red for K faces) in order to let the observer immediately appreciate the surface character of all {hkl} forms. It ensues that, at this calculation level, the F faces do not control the ES as in the case of other molecular crystals.^{11,12} As a matter of fact, among the main crystallographic forms, besides the F ones ({001}, {112}, {010}, and {011}) it is possible to observe a few wide S forms ({11 $\bar{1}$ }, {11 $\bar{3}$ }, {021}). It is noteworthy pointing out that the K forms are not negligible, even if they just appear as tiny connecting facets between F or S surfaces.

In addition, we evaluated the morphological relevance index (MRI)¹¹ for all the {hkl} forms, since it gives an immediate and quantitative estimation of the abundance of the crystallographic forms belonging to the crystal habit, and then a basis to understand the interactions between the crystal and its surroundings.

4.1.2. Sexithiophene (6T). It is possible to identify 5 vdW strong interactions (Table 4 and Figure 1b) and 10 PBCs in the 6T crystal structure. Table 5 shows that the existing PBCs belong to three different classes: three to the first, two to the second, and five to the third PBC rank.

Twenty-three crystallographic forms are generated by the aforementioned PBCs; in detail, 3 are F, 11 are S, and 9 are K forms (see Table 6). The γ_{hkl} difference between relaxed and

Table 4. The Molecular Interactions Issued from the First Bond Order in 6T^a

molecule	molecule in the shifted cell	distance [Å]	direction	interaction [kJ/mol]	bond name
1, 3	2, 4	4.924	[0 0 0]	-81.6	a
1, 3	2, 4	4.975	[0 0 $\bar{1}$]	-81.6	b
1, 2, 3, 4	1, 2, 3, 4	6.029	[0 0 1]	-61.1	c
1, 2	4, 3	23.155	[0 $\bar{1}$ 0]	-8.7	d
1, 2	4, 3	23.042	[1 1 1]	-8.4	e

^aThe calculations were performed by means of program-potential CSEHP-UNI.

bulk-like surfaces in sexithiophene is generally small, with the significant exception of {100}; in this case the Δ_{UR} reaches the absolute value of 15.9%, as a consequence of the highest degree of rearrangement of surface molecules registered by us inside the acenes and oligothiophenes families. Figure 3 contains the sexithiophene equilibrium shapes; they are characterized by a nearly barrel-like habit and a lower morphological variability, if compared to 4T. The bulk-like and relaxed 6T morphologies are mutually similar; however, comparing them to the quaterthiophene case, the two shapes differ more due to the significant relaxation suffered by the {100} form, which tends to flatten the crystal habit.

Table 5. PBC end chain energies (ECEs) relative to the First Bond Order Intermolecular Interactions in 6T^a

PBC	PBC rank	bonds	ECE [erg/molecule]
[0 0 1]	1	a + b + c + d + e	-1.89 × 10 ⁻¹²
[0 1 0]	1	a + b + d + e	-8.46 × 10 ⁻¹³
[0 1 1]	1	a + b + d + e	-3.62 × 10 ⁻¹³
[1 0 1]	2	a + e	-4.80 × 10 ⁻¹⁴
[1 0 2]	2	a + b + d + e	-3.08 × 10 ⁻¹⁴
[2 1 5]	3	a + b + d + e	-1.73 × 10 ⁻¹⁴
[0 1 3]	3	a + b + c + d + e	-1.49 × 10 ⁻¹⁴
[1 1 1]	3	a + e	-9.81 × 10 ⁻¹⁵
[1 1 3]	3	a + d	-3.27 × 10 ⁻¹⁵
[1 0 3]	3	a + d	-2.54 × 10 ⁻¹⁵

^aThe “bonds” column shows the name of the intermolecular bonds forming the PBCs.

Figure 3 reveals, furthermore, that the main forms do not have only the F character; besides the flat {100}, {21̄}, and {110} surfaces, the final models present also the stepped {31̄} and {010} ones, in addition to a few minor K forms (e.g., {30̄} and {43̄}).

4.2. The Growth Shape (GS). Using the same modeling tools, we calculated the attachment energies relative to the crystallographic forms presented in the previous paragraphs.

Tables 3 and 6 show the $E_{\text{att}}^{\text{hkl}}$ concerning 4T and 6T, respectively; the last column of each table reports the $E_{\text{att}}^{\text{hkl}}$ changes due to surface relaxation, that we estimated by the quantity $\Delta_{\text{EAR}} = (E_{\text{att}}^{\text{relaxed}} - E_{\text{att}}^{\text{unrelaxed}})/E_{\text{att}}^{\text{unrelaxed}}$. Δ_{EAR} values are always lower than the Δ_{UR} ones, reaching a maximum of 3.1% considering both crystals.

Figure 4 gives the E_{att} morphologies³⁸ of 4T and 6T, using data in Tables 3 and 6. A first striking feature is the growth

habit fairly different from the equilibrium one: it is definitely more tabular, particularly in 6T, and dominated by the 4T {001} and 6T {100} F forms. This comes as no surprise for these two forms share the same structural motif; in fact, the 4T d_{002} and the 6T d_{200} monomolecular layers enclose the typical herringbone molecular packing of this family of compounds⁴⁰ (the apparent swap of Miller indexes is an effect of the original unit cells choice; the longest parameter c_0 in 4T and a_0 in 6T (see paragraph 4.1) is that of the stacking of herringbone layers). By considering the increased length of the 6T molecule with respect to 4T it is also easy to understand the increased growth anisotropy through its effect on the $E_{\text{att}}^{\text{hkl}}$ and ECE values of the pertinent herringbone layers.

Moreover, the number of crystallographic forms in the growth shape is definitely smaller with respect to the equilibrium one, since no minor rounding faces are present. Only five forms enter the final growth morphology of quaterthiophene: {001}, {011}, {110}, {10̄2}, and {100}; their MRIs, including surface relaxation, are 61.8, 17.0, 12.9, 6.9, and 1.3%, respectively. The sexithiophene GS again includes five forms, namely, {100}, {120}, {30̄}, {21̄}, and {10̄1}, with MRIs equal to 84.0, 7.9, 4.2, 2.9, and 1.1%, respectively. Percentages like these clearly demonstrate that the pinacoid belonging to the heavier oligomer weighs more than in the other smaller oligothiophene, as can be deduced also from the flattening of the crystal shape. As an example of experimental crystal morphology, we report in Figure 5 a 4T crystal grown from a methoxybenzene solution at low supersaturation. The agreement is good, the major elongation axis being [100] as in the predicted growth morphology, although the crystal in Figure 5 and others grown in the same solvent exhibit {100} and {10̄2} forms of negligible area due to their fast growth.

Table 6. Sexithiophene Specific Surface and Attachment Energies for the 23 Crystallographic Forms Arising from First Bond Order Interactions^a

character	form	$\gamma_{\text{unrelaxed}}$	γ_{relaxed}	$\Delta_{\text{UR}} (\%)$	$E_{\text{att}}^{\text{unrelaxed}}$	$E_{\text{att}}^{\text{relaxed}}$	$\Delta_{\text{EAR}} (\%)$
F ₁	{1 0 0}* [*]	87.5	73.6	-15.9	-12.4	-12.5	0.3
S ₃	{3 1 1̄}* [*]	116.1	112.4	-3.2	-158.4	-158.3	0.0
S ₂	{0 1 0}* [*]	117.2	113.1	-3.5	-196.9	-196.0	-0.4
F ₂	{2 1 1̄}* [*]	120.0	115.6	-3.7	-159.8	-159.6	-0.2
S ₃	{4 1 1̄}	120.3	115.6	-3.9	-164.4	-164.5	0.1
S ₃	{1 2 0}* [*]	118.4	115.5	-2.4	-195.2	-194.5	-0.4
F ₃	{1 1 0}* [*]	122.3	117.9	-3.6	-108.8	-108.9	0.2
K ₃	{4 3 1̄}* [*]	127.4	123.8	-2.8	-246.8	-251.2	1.8
S ₃	{3 2 1̄}	128.0	123.8	-3.3	-206.8	-208.8	1.0
S ₃	{2 3 1̄}	128.6	124.8	-3.0	-247.0	-251.5	1.8
K ₃	{3 3 1̄}	129.4	125.3	-3.2	-248.0	-252.9	2.0
K ₃	{6 3 1̄}	129.3	125.7	-2.8	-249.4	-253.9	1.8
K ₃	{1 3 1̄}	130.0	126.9	-2.4	-246.9	-250.5	1.4
S ₂	{1 1 1̄}	133.6	129.5	-3.1			
K ₃	{0 3 1}	133.9	130.7	-2.4	-249.9	-253.5	1.4
K ₃	{3 0 1̄}* [*]	139.1	132.3	-4.9	-150.0	-149.7	-0.2
S ₃	{1 2 1̄}	137.9	132.9	-3.6			
S ₃	{0 1 1}	138.8	133.7	-3.7	-166.9	-166.9	0.0
K ₃	{8 1 3̄}	140.8	136.0	-3.4	-249.4	-254.6	2.1
K ₃	{2 3 1}	140.5	136.6	-2.8	-253.1	-257.7	1.8
K ₃	{5 0 2̄}	144.3	138.4	-4.1	-240.4	-245.2	2.0
S ₂	{2 0 1̄}	148.5	142.0	-4.4	-187.4	-188.4	0.5
S ₂	{1 0 1̄}	162.5	155.6	-4.2	-161.1	-161.0	-0.1

^aValues are calculated by means of UFF, expressed respectively in erg/cm² and kJ/mol, and ordered by relaxed γ values. The boxes with no results indicate calculations that did not reach convergence. Forms with MRI $\geq 1.0\%$ are quoted with an asterisk.

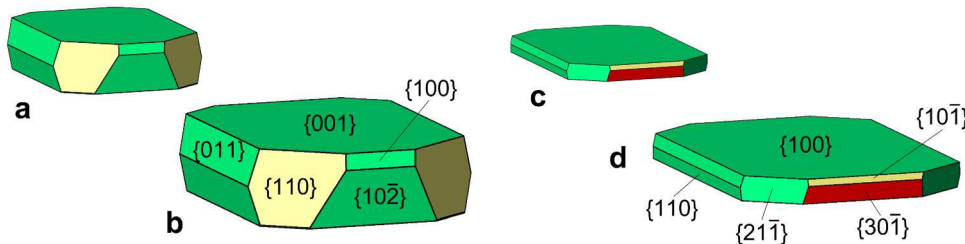


Figure 4. Quaterthiophene and sexithiophene growth shapes from calculations performed by means of UFF. (a) and (b) show the 4T un- and relaxed GS, (c) and (d) the 6T un- and relaxed GS, respectively. Indexes are reported only for those crystallographic forms having $\text{MRI} \geq 1.0\%$.

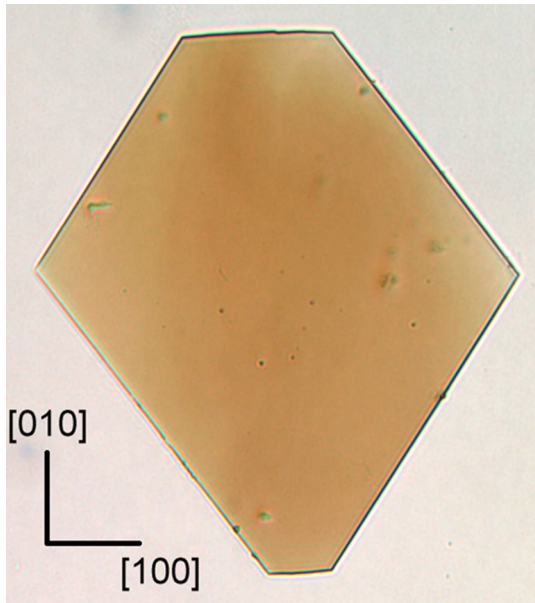


Figure 5. Quaterthiophene single crystal (ca. $2.5 \times 3.0 \times 0.2 \text{ mm}^3$) grown from methoxybenzene solution.

Furthermore, compared to the theoretical growth morphology, true crystals are systematically thinner, with extreme aspect ratios up to the limit of thin (001) flakes.^{41,42}

Our systematic PBC analysis for predicting crystal morphologies can be extended to estimate the shape of 2D nuclei on the basal faces through the calculation of step free energy and attachment energy of a single molecule at a step.⁴³ The Wulff's theorem can be applied to the shape of the 2D critical nucleus by assuming that its equilibrium (growth) shape is determined by the specific edge energies $\rho_{[uvw]}$ (attachment energy of a molecule E_{att}) of steps parallel to the strongest PBCs on the (hkl) surface. It is worth noting that the shape of growth spiral is determined, in a steady state, by the velocity of propagation of the steps belonging to the equilibrium nucleus. Thus, unrelaxed $\rho_{[uvw]}$ and E_{att} values were calculated, under the assumption of crystal–vapor equilibrium (Table 7). The shape of the 2D nucleus has been obtained by a two-dimensional Wulff's construction for the dominant (basal) faces of 4T and 6T, both growing by spiral mechanism at low supersaturation⁴⁴ (Figure 6). It can be noticed that visually the estimated 2D nucleus shapes for 4T and 6T are indistinguishable due to the very close ratio between step and attachment energies of corresponding PBC directions. Apart from a 60% increase of the $\rho_{[uvw]}$ and E_{att} values for 6T compared to 4T due to the presence of six instead of four rings, the herringbone structures are nearly identical. In Figure 7 are reported experimental

Table 7. Step Energy and Molecular Attachment Energies at Steps for the Strong PBCs Lying in the 4T d_{002} and 6T d_{200} Slices^a

step	$\rho_{[uvw]}$ [erg/cm]	E_{att} [erg/molecule]
4T[1 0 0]	1.75×10^{-5}	-1.95×10^{-12}
4T[0 1 0]	2.18×10^{-5}	-1.64×10^{-12}
4T[1 1 0]	1.81×10^{-5}	-1.69×10^{-12}
6T[0 0 1]	2.82×10^{-5}	-3.09×10^{-12}
6T[0 1 0]	3.55×10^{-5}	-2.65×10^{-12}
6T[0 1 1]	2.95×10^{-5}	-2.73×10^{-12}

^aValues calculated by means of UNI potential.

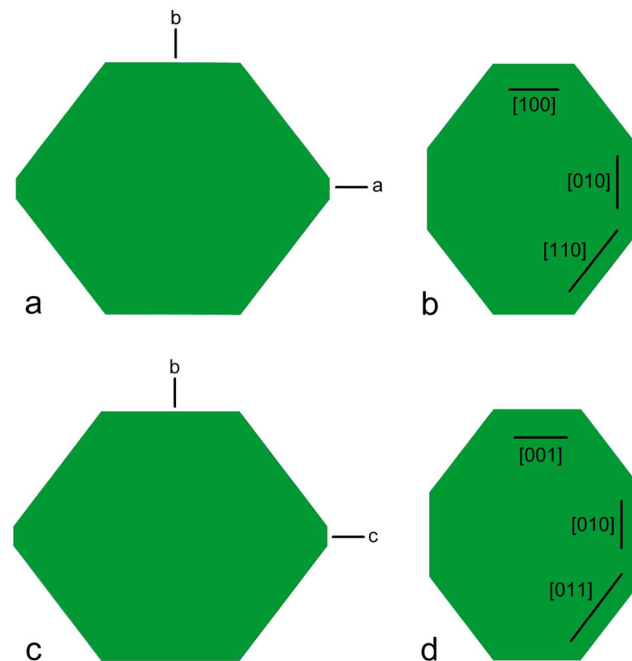


Figure 6. Shape of the two-dimensional nucleus calculated by means of UNI potential. Equilibrium (a) and growth (b) shape for 4T{001}, equilibrium (c) and growth (d) shape for 6T{100}.

growth features observed for 4T(001) and 6T(100) faces characterized by the presence of large growth hillocks. As it can be seen, the experimental spiral shapes are quite close to that of the calculated 2D nucleus, with an elongation ratio which does agree with the observed one. Although many other factors such as solvent adsorption on the edges (growth was from anisole solutions in Figure 7a,b) and/or surface and volume diffusion of solute molecules are potentially able to alter the observed features compared to the calculated ones, the agreement is good.

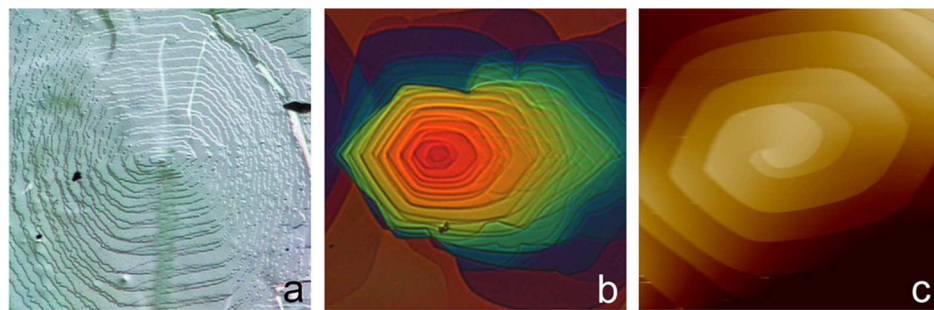


Figure 7. Growth hillocks for (a) (001) face of a 4T crystal grown from methoxybenzene solution⁴² (differential interference microscopy, size $250 \times 250 \mu\text{m}^2$); (b) (100) face of a 6T crystal grown from methoxybenzene solution⁴² (differential interference microscopy image, size $300 \times 300 \mu\text{m}^2$); (c) (100) face of a 6T crystal grown by physical vapor transport under nitrogen flow⁴¹ (atomic force microscopy image, size $60 \times 60 \mu\text{m}^2$).

Table 8. In the Upper Part the MRIs $\geq 1.0\%$ of 4T and 6T resulting from the First Bond Order Calculation Are Shown^a

MRI (%)	34.1 {001}		38.1 {100}							
	34.2 {001}	15.0 {11̄1}	20.9 {31̄1}	15.7 {21̄1}	42.1 {100}	61.9 {001}	61.8 {001}	84.0 {100}	84.0 {100}	
	16.5 {11̄1}	14.4 {11̄3}	7.5 {120}	18.4 {31̄1}						
	14.9 {11̄3}	10.4 {11̄2}	4.8 {110}	18.2 {21̄1}	61.0 {011}	17.0 {011}	7.9 {110}	7.9 {110}		
	9.5 {11̄2}	7.8 {021}	3.4 {010}	6.7 {010}	12.9 {110}	12.9 {110}	4.2 {21̄1}	4.2 {21̄1}		
	8.0 {021}	4.7 {011}	2.4 {011}	6.4 {110}						
	4.6 {011}	3.2 {010}	1.5 {13̄1}	2.1 {120}	6.9 {10̄2}	6.9 {10̄2}	2.8 {30̄1}	2.9 {30̄1}		
	3.5 {010}	2.3 {111}	1.3 {63̄1}	1.7 {30̄1}	1.3 {100}	1.3 {100}	1.2 {10̄1}	1.1 {10̄1}		
	3.0 {111}	1.5 {110}	1.2 {41̄1}	1.0 {43̄1}						
	1.6 {13̄2}	1.4 {13̄2}	1.0 {43̄1}							
		1.0 {10̄2}	1.0 {30̄1}							
shape phase relaxation	equilibrium				growth					
	4T		6T		4T		6T			
	no	yes	no	yes	no	yes	no	yes		
PBC 1	34.2%	34.1%	38.1%	42.1%	61.9%	61.8%	84.0%	84.0%		
PBC 2	65.8%	65.9%	19.3%	25.1%	38.1%	38.2%	5.3%	5.3%		
PBC 3	-	-	42.6%	32.8%	-	-	10.6%	10.7%		
F	52.6%	53.3%	58.6%	66.7%	87.1%	87.1%	96.1%	96.1%		
S	42.7%	41.3%	36.1%	29.0%	12.9%	12.9%	1.2%	1.1%		
K	4.7%	5.4%	5.3%	4.3%	-	-	2.8%	2.9%		

^aIn the lower part the total MRI referred to PBC categories and to the character of the faces. All data were calculated with UFF.

Table 8 summarizes all the equilibrium and growth morphology data about the oligothiophenes studied. It gives details about the MRI of all forms with surface extension $\geq 1.0\%$ for the two phases; the weight of the character and the pertinent PBC rank are reported as well. This table supports some important conclusions:

(i) The 4T {001} and the 6T {100} are absolutely the dominant forms in every final morphology, with MRIs near 35% and 62% for quaterthiophene ES and GS, and near 40% and 84% for sexithiophene ES and GS, respectively;

(ii) The forms arising from the first PBC rank control the final growth shapes, their MRI never going below about 62% and 84%, respectively for 4T and 6T;

(iii) The F character is even more leading in the GS, the relative MRIs being near 87% and 96% for 4T and 6T, respectively; K faces are completely lacking in 4T, but wider than S faces in 6T;

(iv) The first PBC rank faces lose importance in controlling the final equilibrium shapes; in detail, the second PBC rank faces prevail in 4T with an MRI of 66%, while the three different characters are more similar in 6T, with the following order of abundance: F, K, S;

(v) The F equilibrium forms do not lead as in the GS; they codominate with the S forms, the K ones having always a value near 5%. The importance of the F character is more relevant in 6T, and this is more true if surface relaxation is considered.

5. CONCLUSIONS

We performed a morphological study about two members of the oligothiophenes class, definitely confirming some results achieved in a couple of recent papers about acenes.^{11,12} The equilibrium and growth shapes obtained from our simulations are richer in crystallographic forms compared to those recently appearing in the literature.^{18–22} This is because we carry out a

thorough PBC analysis, instead of applying the arbitrary assumption that only low index surfaces enter the final morphology of crystals. Moreover, we observed that surface relaxation weakly affects surface (apart from the sexithiophene {100}) and, even less, attachment energies of molecular crystals; this phenomenon is far from what we observed in recent years with ionic crystals.^{45–48}

As seen with acenes,^{11,12} crystalline oligothiophenes have many forms with similar specific surface energies. This implies that the equilibrium morphologies are densely faceted and strongly influenced by the point group symmetry: the predicted ES (but also the GS) of 4T and 6T, which belong to the monoclinic prismatic class 2/m, are very similar. The equilibrium habits result to be rather barrel-like: one form, the {001} for quaterthiophene and the {100} for sexithiophene, rules over the other ones and several faces roughly belong to the zone axis perpendicular to the dominant form. Similarly to the acenes, the calculated crystal shapes, above all the GS, reveal that oligothiophenes crystals are strongly influenced by the structural arrangement of their herringbone packing motif. Invariably, all the predicted GS turn out to be flattened according to the pinacoid form, the 4T d_{002} and the 6T d_{200} containing the highly compact herringbone packing. In terms of the Hartman–Perdok theory, this means that a form could dominate the final growth habit if its d_{hkl} includes several and, possibly, strong periodic boundary chains, and this is even more evident for the heavier oligomer which owns the longest polycyclic core.

AUTHOR INFORMATION

Corresponding Author

*E-mail: roberto.massaro@mater.unimib.it.

Notes

The authors declare no competing financial interest.

REFERENCES

- (1) Braga, D.; Horowitz, G. *Adv. Mater.* **2009**, *21*, 1473–1486.
- (2) de Boer, R. W. I.; Gershenson, M. E.; Morpurgo, A. F.; Podzorov, V. *Phys. Status Solidi* **2004**, *201*, 1302–1331.
- (3) Podzorov, V.; Menard, E.; Borissov, A.; Kiryukhin, V.; Rogers, J. A.; Gershenson, M. E. *Phys. Rev. Lett.* **2004**, *93*, 086602.
- (4) de Boer, R. W.; Klapwijk, T. M.; Morpurgo, A. F. *Appl. Phys. Lett.* **2003**, *83*, 4345–4347.
- (5) Mas-Torrent, M.; Rovira, C. *Chem. Rev.* **2011**, *111*, 4833–4856.
- (6) Anthony, J. E. *Chem. Rev.* **2006**, *106*, 5028–5048.
- (7) Reese, C.; Bao, Z. *J. Mater. Chem.* **2006**, *16*, 329–333.
- (8) Witte, G.; Wöll, C. *J. Mater. Res.* **2004**, *19*, 1889–1916.
- (9) Lunt, R. R.; Benziger, J. B.; Forrest, S. R. *Adv. Mater.* **2010**, *22*, 3857–3875.
- (10) Moret, M.; Borghesi, A.; Campione, M.; Fumagalli, E.; Raimondo, L.; Sassella, A. *Cryst. Res. Technol.* **2011**, *46*, 827–832.
- (11) Massaro, F. R.; Moret, M.; Bruno, M.; Rubbo, M.; Aquilano, D. *Cryst. Growth Des.* **2011**, *11*, 4639–4646.
- (12) Massaro, F. R.; Moret, M.; Bruno, M.; Aquilano, D. *Cryst. Growth Des.* **2012**, *12*, 982–989.
- (13) Campione, M.; Sassella, A.; Moret, M.; Papagni, A.; Trabattoni, S.; Resel, R.; Lengyel, O.; Marcon, V.; Raos, G. *J. Am. Chem. Soc.* **2006**, *128*, 13378–13387.
- (14) Haber, T.; Resel, R.; Thierry, A.; Campione, M.; Sassella, A.; Moret, M. *Physica E* **2008**, *41*, 133–137.
- (15) Campione, M.; Moret, M.; Raimondo, L.; Sassella, A. *J. Phys. Chem. C* **2009**, *113*, 20927–20933.
- (16) Campione, M.; Raimondo, L.; Moret, M.; Campiglio, P.; Fumagalli, E.; Sassella, A. *Chem. Mater.* **2009**, *21*, 4859–4867.
- (17) Raimondo, L.; Moret, M.; Campione, M.; Borghesi, A.; Sassella, A. *J. Phys. Chem. C* **2011**, *115*, 5880–5885.
- (18) Grimbergen, R. F. P.; Reedijk, M. F.; Meekes, H.; Bennema, P. J. *Phys. Chem. B* **1998**, *102*, 2646–2653.
- (19) Northrup, J. E.; Tiago, M. L.; Louie, S. G. *Phys. Rev. B* **2002**, *66*, 121404.
- (20) Cuppen, H. M.; Graswinckel, W. S.; Meekes, H. *Cryst. Growth Des.* **2004**, *4*, 1351–1357.
- (21) Drummy, L. F.; Miska, P. K.; Alberts, D.; Lee, N.; Martin, D. C. *J. Phys. Chem. B* **2006**, *110*, 6066–6071.
- (22) Nabok, D.; Puschnig, P.; Ambrosch-Draxl, C. *Phys. Rev. B* **2008**, *77*, 245316.
- (23) Hartman, P.; Perdok, W. G. *Acta Crystallogr.* **1955**, *8*, 49–52.
- (24) Hartman, P.; Perdok, W. G. *Acta Crystallogr.* **1955**, *8*, 521–525.
- (25) Hartman, P.; Perdok, W. G. *Acta Crystallogr.* **1955**, *8*, 525–529.
- (26) Siegrist, T.; Kloc, C.; Laudise, R. A.; Katz, H. E.; Haddon, R. C. *Adv. Mater.* **1998**, *10*, 379–382.
- (27) Horowitz, G.; Bachet, B.; Yassar, A.; Lang, P.; Demanze, F.; Fave, J.-L.; Garnier, F. *Chem. Mater.* **1995**, *7*, 1337–1341.
- (28) Campione, M.; Sassella, A.; Moret, M.; Thierry, A.; Lotz, B. *Thin Solid Films* **2006**, *500*, 169–173.
- (29) Campione, M.; Caprioli, S.; Moret, M.; Sassella, A. *J. Phys. Chem.* **2007**, *C11*, 12741–12746.
- (30) Aquilano, D.; Rubbo, M.; Catti, M.; Pavese, A. *J. Cryst. Growth* **1997**, *182*, 168–184.
- (31) Rubbo, M.; Aquilano, D. *J. Cryst. Growth* **1998**, *194*, 156–159.
- (32) Filippini, G.; Gavezzotti, A. *Acta Crystallogr. B* **1993**, *49*, 868–880.
- (33) Gavezzotti, A. *Molecular Aggregation: Structure Analysis and Molecular Simulation of Crystals and Liquids*; Oxford University Press: New York, 2007.
- (34) Rappé, A. K.; Casewit, C. J.; Colwell, K. S.; Goddard, W. A., III; Skiff, W. M. *J. Am. Chem. Soc.* **1992**, *114*, 10024–10035.
- (35) Gale, J. D. *J. Chem. Soc. Faraday Trans.* **1997**, *93*, 629–637.
- (36) Dovesi, R.; Civalleri, B.; Orlando, R.; Roetti, C.; Saunders, V. R. In *Reviews in Computational Chemistry*; Lipkowitz, B. K.; Larter, R.; Cundari, T. R., Eds.; John Wiley and Sons Inc.: New York, 2005; Vol. 21, pp 1–125.
- (37) Gale, J. D. *General Utility Lattice Program User's Manual*; Curtin University of Technology: Perth, Australia.
- (38) Hartman, P.; Bennema, P. *J. Cryst. Growth* **1980**, *49*, 145–156.
- (39) Kern, R. In *Morphology of Crystals Part A*; Sunagawa, I., Ed.; Terra Scientific Publishing Co.: Tokyo, 1987; pp 77–206.
- (40) Fichou, D. *J. Mater. Chem.* **2000**, *10*, 571–588.
- (41) Laudise, R. A.; Kloc, Ch.; Simpkins, P. G.; Siegrist, T. *J. Cryst. Growth* **1998**, *187*, 449–454.
- (42) Campione, M.; Ruggerone, R.; Tavazzi, S.; Moret, M. *J. Mater. Chem.* **2005**, *15*, 2437–2443.
- (43) Aquilano, D.; Rubbo, M.; Mantovani, G.; Sgualdino, G.; Vaccari, G. *J. Cryst. Growth* **1986**, *74*, 10–20.
- (44) Burton, W. K.; Cabrera, N.; Frank, F. C. *Philos. Trans. R. Soc. A* **1951**, *243*, 299–358.
- (45) Bruno, M.; Massaro, F. R.; Prencipe, M. *Surf. Sci.* **2008**, *602*, 2774–2782.
- (46) Bruno, M.; Massaro, F. R.; Prencipe, M.; Aquilano, D. *CrystEngComm* **2010**, *12*, 3626–3633.
- (47) Massaro, F. R.; Bruno, M.; Aquilano, D. *Cryst. Growth Des.* **2010**, *10*, 4096–4100.
- (48) Massaro, F. R.; Rubbo, M.; Aquilano, D. *Cryst. Growth Des.* **2010**, *10*, 2870–2878.